NEUTRON RADIOGRAPHY STUDIES FOR CULTURAL HERITAGE WITHIN THE NEU_ART PROJECT

Roberto SACCHI*

Dipartimento di Fisica Sperimentale, Università di Torino e INFN, Sezione di Torino

Durisi E.[1], Lo Giudice A.[1], Mila G.[1], Re A.[1], Romero A.[1], Visca L.[1], Demmelbauer M.[2], Giovagnoli A.[2], Nervo M.[2], Radelet T.[2,4], Dughera G.[3],Pastrone N.[3], Prino F.[3], Staiano A.[3]

(1) Dipartimento di Fisica Sperimentale, Università di Torino e INFN, Sezione di Torino
(2) Fondazione Centro Conservazione e Restauro "La Venaria Reale"
(3) INFN, Sezione di Torino
(4) Private instrumentation

* sacchi@to.infn.it
keywords: neutrons, radiography, imaging

ABSTRACT
One of the aims of neu_ART project is to investigate the capability of fast neutron imaging applied on artefacts of interest for cultural heritage. Compact systems based on D-D or D-T fast neutron sources could be installed in certificated laboratories near restoration centers as diagnostic tools to plan the restoration work. This paper presents preliminary studies carried out at fast (NECTAR) and thermal (INES) neutron facilities. Custom samples of different thicknesses, internal structures and material compositions were analyzed, together with artistic objects to compare the performance of fast and thermal neutron radiography. We focused our studies on the neutron penetration into metals, as bronze, iron, and brass. A detailed analysis of the results is presented and compared with digital X-ray radiography. These two complementary techniques can be integrated to fully characterize the objects under study.

INTRODUCTION
The imaging potential of cold and thermal neutrons has been assessed in the cultural heritage field. They allow non-destructive analysis [1], can penetrate thick layers of materials and permit to determine the presence of low Z elements within metals. Fast neutrons provide similar information especially when thick or dense materials are involved [2].
At present commercial compact neutron generator based on D-D or D-T fusion reaction are available. They consist mainly of a source to generate positively charged ions, one or more structures to accelerate the ions (usually the acceleration voltage lies between 100 kV – 400 kV), a metal hydride target loaded with deuterium, tritium, or a mixture of the two. These generators provide fast neutrons (2,5 MeV or 14 MeV when D-D or D-T reactions are used respectively) and reasonable neutron yield [3]. Feasibility studies are in progress within the framework of the regional project neu_ART [4] to assess and better exploit the capabilities of these neutron sources.
This paper presents a preliminary work focused on the comparison of fast and thermal neutron radiography technique applied on different artistic handworks. The results are also compared with digital X-ray radiographies, which provide complementary information on the inner structure of the artefacts.

1 METHODS
1.1 Physics
The dominant interaction of a neutron beam penetrating the matter is with the atomic nuclei. The total microscopic neutron cross section of each element is related to the interaction probability and is a function of the neutron energy. As it is shown in Figure 1 (left) the cross section decreases steadily

with increasing energy up to about 100 eV (absorption region). Then it rises sharply to high values called resonance peaks at energies corresponding to excited nucleus states. Neutron cross sections may be very different among nuclei even with close atomic number.

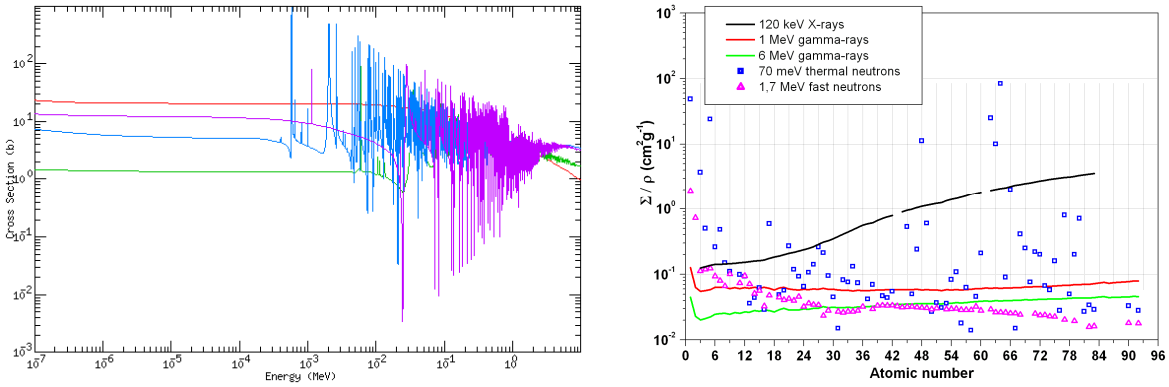

Fig. 1: Total neutron microscopic cross sections (L) and elemental mass attenuation coefficients (R).

The measured intensity I of a transmitted neutron parallel beam through a layer of material with thickness x is related to the incident intensity I_0 according to the inverse exponential law:

$$I = I_0 e^{-\Sigma x} \tag{1}$$

The macroscopic cross section Σ depends on the microscopic cross section σ, the material density ρ, the atomic number A and Avogadro's number N_A:

$$\Sigma = \rho\sigma\frac{N_A}{A} \tag{2}$$

Σ^{-1} indicates the material thickness required to attenuate the beam by 1/e=37%. The same formula is used to describe the X-ray penetration through matter. X-ray interact with atomic electrons so their cross section increases smoothly with the atomic number Z. Fig. 1 (right), computed using ENDFB-VI library for neutrons and NIST data for X-ray, compares the mass attenuation coefficients (Σ/ρ) for X-ray, thermal and fast neutrons at different energies. The behavior of 120 keV X-ray and fast neutrons is complementary for elements with high atomic number.

Experimentally, mass attenuation coefficients can be computed by taking radiographs of step wedges. Based on the known thickness x of each step and the measured intensity of the transmitted beam I, the data can be fitted with the function (derived from Eq. 1):

$$\ln(I) = \ln(I_0) - \Sigma x \tag{3}$$

The slope divided by the material's density gives mass attenuation coefficient.

1.2 Image processing

1.2.1 Image resolution

The spatial resolution of an isotropic optical system can be computed starting from a sharp edge radiography [5]. It is function of the edge profile width, as shown in Fig. 2.

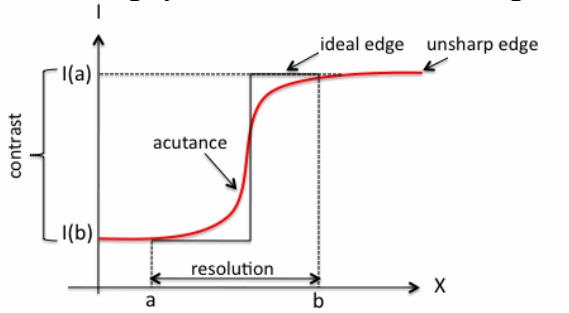

Fig. 2: Schematic picture of a sharp edge profile.

The fit of the rising edge is performed using the Cauchy formula (Edge Spread Function):

$$ESF = f(x) = a\left\{\frac{1}{2} + \frac{1}{\pi}\arctan[\lambda(x - x_0)]\right\} + b \tag{4}$$

where λ is the width parameter, x_0 the theoretical position of the edge, a and b constants. Spatial resolution R is defined as:

$$R = \frac{2}{\lambda} \tag{5}$$

Alternatively the evaluation can be performed by calculating the Modular Transfer Function (MTF), derived from ESF's derivative by Fourier transformation:

$$MTF = \int_{-\infty}^{+\infty} f'(x) \cdot e^{-2\pi i \xi x} dx = \int_{-\infty}^{+\infty} \left[\frac{\lambda}{\pi}\frac{1}{1+(\lambda x)^2}\right] \cdot e^{-2\pi i \xi x} dx = e^{-\frac{2\pi}{\lambda}\xi} \tag{6}$$

The spatial resolution is defined as the MTF value at 10% and it is expressed in line pairs per millimeter (lp/mm).

1.2.2 Image reconstruction

During neutron radiography measurements a relatively large number of scattered gamma rays hit the CCD chip. This results in a contribution of randomly distributed signals in individual pixels. Thus for each radiography, a number of frames are acquired which are later processed with a 3x3 median filter and the resulting images are summed up.

The final radiography (I_F) is obtained after dark image (*D.I.*) subtraction and normalization for the beam image (*B.I.*):

$$I_F = \frac{\sum_{i=1}^{n} I_i - \sum_{i=1}^{n} D.I._i}{\sum_{i=1}^{n} B.I._i - \sum_{i=1}^{n} D.I._i} \tag{7}$$

Fig. 3 shows an example of the frames used for the image reconstruction process.

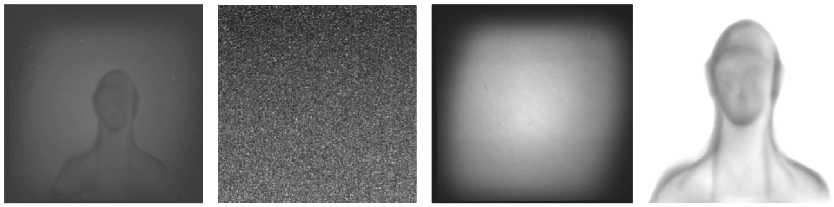

Fig. 3: From left to right: a raw frame, the dark and the beam images and the final radiograph.

3 FAST NEUTRON RADIOGRAPHY

3.1 Experimental setup

The NECTAR (NEutron Computerized Tomography And Radiography) facility [6] is located at FRM-II laboratory, which is equipped with a fission neutron source. Two thermal-to-fast neutron converter plates containing highly enriched uranium are placed in the moderator tank in a distance of about 1m from the reactor core.

The facility consists of collimators, a 3D manipulator to handle the sample and detector systems.

The first collimator is mainly composed of cadmium to suppress thermal neutrons and lead for reducing the high gamma-radiation background created by the fission process in the converter plates. It is coupled with an iron collimator to improve the L/D value up to 300 with a neutron flux at the sample position of $5.4 \times 10^{+05}$ $cm^{-2}s^{-1}$ and mean energy of 1.7 MeV. The beam transverse size is 37x31 cm^2.

The sample manipulator is composed by a three-axis motor to lift, translate and rotate objects in a volume of 80x80x80 cm^3.

Neutron are detected and converted into visible light by a scintillating screen of ZnS(Ag) embedded in plastic with low sensitivity to gamma-radiation. Neutron radiographies are recorded by a thermoelectric cooled CCD camera (ANDOR DV434-BV) having a maximum detection area of 30x30 cm^2 with an array of 1024x1024 60 µm pixels and a 16-bit dynamic range.

3.2 Spatial resolution (MTF)

An appropriate Region Of Interest (ROI) of a NECTAR frame (Fig. 4, left) has been chosen to evaluate the resolution of the radiographic system. Its gray level profile is shown in the right part of Fig. 4 using the method explained in Section 1.2.1. The computed spatial resolution is (0.568±0.005) mm which corresponds to 1.29 lp/mm in the MTF computation.

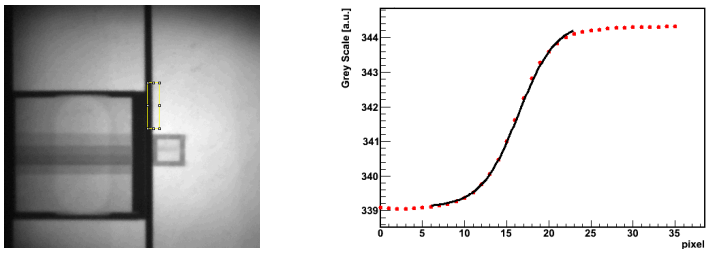

Fig. 4: NECTAR radiograph, ROI (L) and profile (R) used for the spatial resolution computation.

3.3 Material composition

Three step wedges have been used to compute the attenuation coefficients of three metals alloys (iron, brass and bronze) widely used in ancient and modern artefacts. The depth of each step increases by 2 mm, up to 30 mm. Fig. 5 shows a picture of the wedges and the corresponding neutron radiography. Since the fast neutron cross sections of these materials are very similar, the elemental separation is not clearly visible in the radiograph.

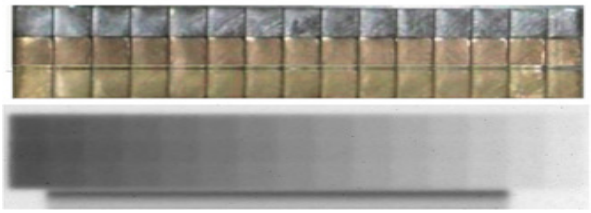

Fig. 5: Iron (T), bronze (C) and brass (B) step wedges: photo and NECTAR neutron radiography.

Fig. 6 illustrates on the left side the profile of the intensity values derived from the neutron radiograph and on the right side the histogram used for the mass attenuation coefficient computation, as explained in Section 1.1, Eq. 3. The result is (0.0320 ± 0.0003) g/cm^2 for iron, (0.0306 ± 0.0002) g/cm^2 for brass and (0.0297 ± 0.0002) g/cm^2 for bronze.

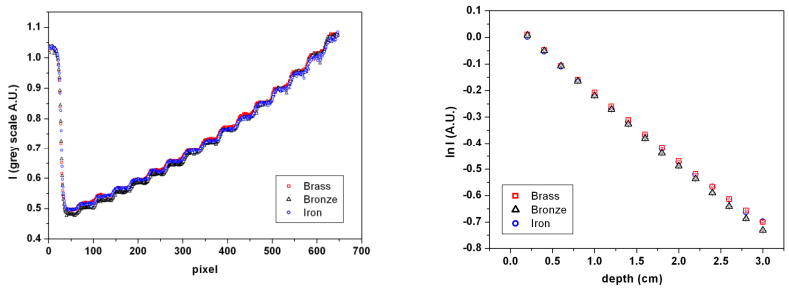

Fig. 6: Gray scale values for three step wedges (L), as function of material depth (R) – NECTAR data.

3.4 Results on fake statues in Etruscan style

Radiographies of two samples of fake Etruscan statues (Figure 7) have been performed in order to exploit the analysis potential of fast neutron imaging. The presence of organic residuals, which are strongly interacting with neutrons, is highlighted in the statue arm. They are probably tied to the ancient melting method and restorers suggest that this arm could be the single original part of the artefact. Moreover the neutron radiography shows a welting region on the left calf which is not visible from the external part of the statue. The mirror resulted filled with a homogenous layer of metals. Restorers were interested mostly in the fastening with the turtle pedestal, which ensures the artefact stability.

Fig. 7: NECTAR radiographies of two fake Etruscan artefacts.

4 THERMAL NEUTRON RADIOGRAPHY

4.1 Experimental setup

The Italian Neutron Experimental Station (INES) is located at ISIS [7,8]. Here, neutrons are produced by pulsed proton bunches hitting a tantalum target. The main component of the incident flux is epithermal neutrons, while thermal and cold neutrons represent the Gaussian tail of the beam spectrum. The INES sample position is located at L=23.84 m from the neutron source where the collimation system allows an effective size of the beam source of 8.5 cm and a beam section of 4.4x4.4 cm^2.

Neutrons transmitted through the sample reach a converter screen made of ZnS/^{6}LiF layered on an aluminum substrate. The scintillator plate is tilted 45° with respect to the incident neutron beam, with an average distance from the sample of 10 cm. It emits on visible light centered at $\lambda \approx 520\mu m$.

A X-Y stepper motor provides the sample handling.

The scintillator screen is observed by a commercial black and white CCD camera (The Imaging Source DMK21BF04) equipped with a optical system (f=8 mm and F=1.4). The camera works at a room temperature without any image intensifier. The CCD sensor has 640x480 pixels of size 5.6x5.6 μm^2 and it is equipped with a 10 bit ADC whose most significant 8 bit are the output signal.

4.2 Spatial resolution (MTF)

The same procedure for the image resolution computation of NECTAR neutron radiographs (Sec. 3.2) has been applied on INES data. The neutron radiograph, the ROI and its profile used for this purpose are shown in Fig. 8. The resulting spatial resolution is (0.484±0.008) mm corresponding to 1.51 lp/mm.

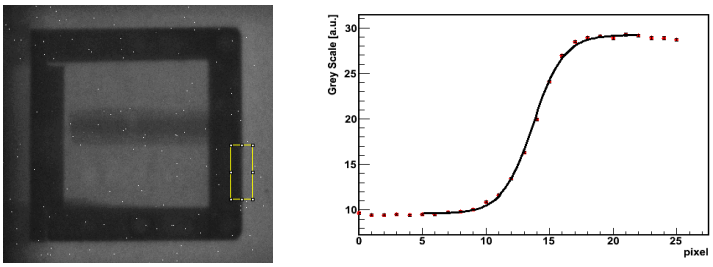

Fig. 8: INES radiograph, ROI (L) and profile (R) used for the spatial resolution computation.

4.3 Material composition

The three step wedges used at the NECTAR facility have been also studied into the INES station. Fig. 9 shows the neutron radiography. Compared to the images obtained at NECTAR, a better separation among the intensity values of the different materials is seen. This reflects the neutron cross sections being much different for the three materials for thermal neutrons than for fast neutrons.

Fig. 9: INES neutron radiograph of a step wedge made of (from top to bottom) brass, iron and bronze.

Fig. 10 illustrates the profile of the intensity values on the left side and the plot used for the mass attenuation coefficient computation, on the right side. The result is (0.1127 ± 0.0008) g/cm^2 for iron, (0.0589 ± 0.0008) g/cm^2 for brass and (0.0697 ± 0.0009) g/cm^2 for bronze.

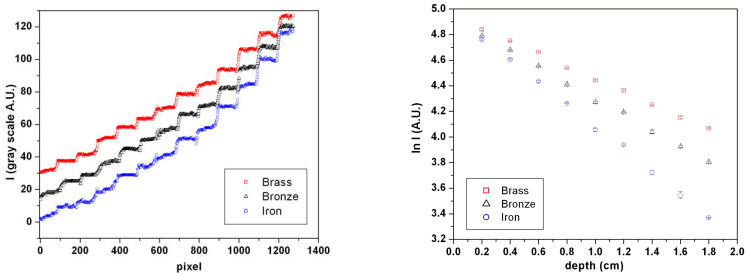

Fig. 10: Gray scale values for three step wedges (L), as function of material depth (R) – INES data.

4.4 Results on fake statues in Etruscan style

Radiographs of the most interesting parts of the fake Etruscan statue and mirror have been performed with the INES experimental set-up, as illustrated in Fig. 11. These images, which show a better resolution for small details than the NECTAR ones, confirm the results of Section 3.4.

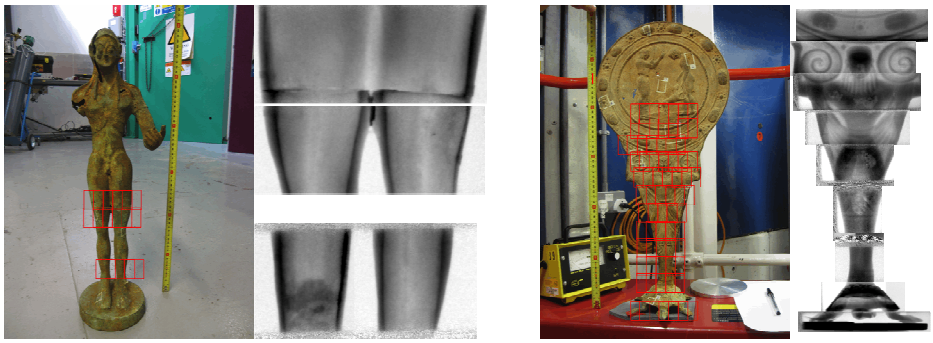

Fig. 11: INES radiographies of two fake Estruscan artefacts

5 X-RAY RADIOGRAPHY

5.1 Experimental setup

The experimental instrumentation [9] consists mainly in a X-ray source, a set of photographic plates, a digital scanner and a portable computer.

The source is a CP120 X-ray tube with a localize spot from 0.5 to 0.25 mm. The beam opening is 60x40 degree. It is able to work up to 120 kV voltage and 1mA anodic current. An aluminum filter, 4 mm thickness, is used for the beam hardening.

The plates are made of phosphorus crystals and their size is 35x43 cm^2.

The scanner develops the plates using a digitalization step up to 25μm with 60 megapixel resulting images for each radiograph. It can make use of 64000 grey levels.

5.2 Spatial resolution (MTF)

The linear side of the bronze step wedge has been used to compute the experimental spatial resolution, according to the method outlined in Sec. 3.2. Fig. 12 shows the X-ray radiograph, the ROI and its grey level profile. The image resolution results in (0.199±0.004) mm, corresponding to 3.68 lp/mm.

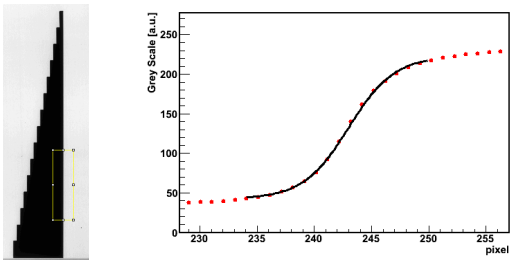

Fig. 12: X-ray radiograph, ROI (L) and profile (R) used for the spatial resolution computation.

5.3 Material composition

The radiograph of the three step wedges made of bronze, brass and iron is shown in Fig. 13. It is clearly visible that the X-ray are completely absorbed after the first six steps, corresponding to 12 mm thickness. This is due to the X-ray absorption cross section in metals being much larger than for a neutron beam.

Fig. 13: X-ray radiograph of a step wedge made of bronze, brass and iron (top to bottom).

Fig. 14 shows the grey levels profiles (left) and the intensity values as a function of the material thickness (right). The expected logarithmic behavior is present only in the first two-three steps, then saturation effects appear for steps with higher thicknesses. From the interpolation of the first wedges, the mass attenuation coefficients results in (0.450 ± 0.009) g/cm^2 for iron, (0.541 ± 0.011) g/cm^2 for brass and (0.609 ± 0.012) g/cm^2 for bronze.

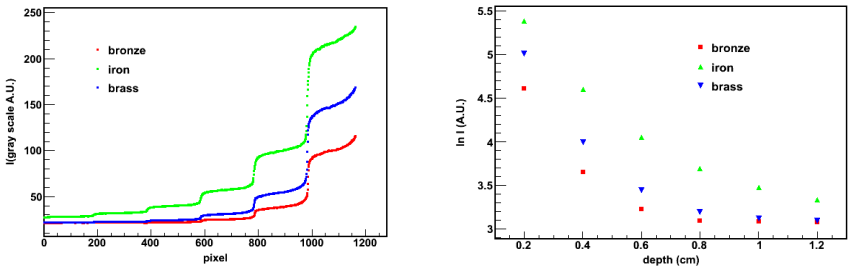

Fig. 14: Gray scale values for three step wedges (L), as function of material depth (R) – X-ray data.

5.4 Results on fake statues in Etruscan style

The radiographs of the fake Etruscan statue and mirror (Fig. 15, left) show the complementary analysis potential of X-ray respect to neutrons. X-ray clearly have a higher potential in resolving small details, as shown in Fig. 15, right. However they are not sensible to the presence of organic elements inside metals. Moreover X-ray can highlight differences in the material thickness but only up to 8mm.

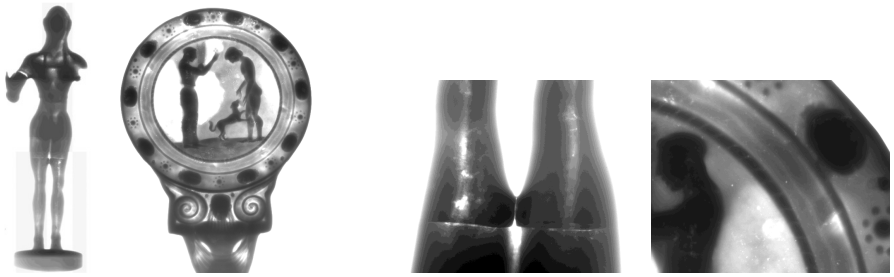

Fig. 15: X-ray radiographies of two fake Estruscan artefacts.

CONCLUSIONS

Preliminary studies on neutron imaging of cultural heritage samples have been carried out with fast and thermal neutrons at NECTAR and INES facilities. The aim of this work is to explore capabilities and limits of these sources in order to evaluate the possible application of D-D or D-T neutron compact generators. Moreover, the same custom samples and artefacts have been analyzed with X-ray radiography, as a complementary diagnostic technique.

Spatial resolution and intensity profiles as functions of depth and type of material have been determined using dedicated mechanical wedges, in order to compare thermal and fast neutron imaging, and finally with X-ray imaging characteristics.

Thermal neutrons can highlight differences between metals better than fast neutrons. However, fast neutrons can cross a higher material thickness. X-ray radiography provides a better resolution compared to the neutron beams used in this study, but in contrast to the neutron inspection, it is not sensitive to the presence of organic elements inside metals.

In conclusion, thermal and fast neutrons, together with X-ray, provide complementary information which can be used to fully characterize the artefacts. The choice of the best imaging technique is strictly related to the characteristics (material, shape, dimensions) of the handwork and depends on the diagnostic information which are desired.

ACKNOWLEDGEMENTS

This work was supported by the Regional Project neu_ART (Bando Scienze Umane e Sociali 2008) of the Regione Piemonte (Italy). The authors would like to thank Dr. Thomas Bücherl (Lehrstuhl fur Radiochemie, Technische Universitat Munchen, Germany) at NECTAR and Dr. Francesco Grazzi (CNR, Istituto dei Sistemi Complessi, Italy) and Antonella Scherillo (STFC, ISIS Neutron Source, UK) at INES for the precious advices and the support during the measurements.

REFERENCES

[1] E. Lehmann et al., “Non-invasive studies of objects from cultural heritage”, Nuclear instruments & methods in physics research. Section A, ISSN 0168-9002.

[2] T. Bucherl et al., “Radiography and tomography using fission neutrons the NECTAR facility”, Nuclear Science Symposium Conference Record (NSS/MIC), 2009 IEEE.

[3] D.L. Chichester et al., “The API 120: A portable neutron generator for the associated particle technique”, Nuclear Instruments & Methods in Physics Research B 241 (2005) 753–758.

[4] http://neuart.to.infn.it

[5] Hall, Ernest L., “Computer image processing and recognition”, Academic Press, 1979-XVII, 584 p.

[6] T. Bucherl et al., Proceeding of 2006 International Workshop on Fast Neutron Detectors and Applications, University of Cape Town, South Africa, April 3-6, 2006.

[7] F. Grazzi et al., Nuovo Cimento C 30, 59 (2007).

[8] F. Grazzi et al., “A neutron imaging device for sample alignment in a pulsed neutron scattering instrument”, Review of Scientific Instruments 80, 093704 1-4 (2009).

[9] T. Radelet, “La radiografia digitale applicata a *Il Quarto Stato* di Pelizza da Volpedo”, Kermes - La rivista del restauro.